Double-layered nitrocellulose membrane sample holding technique for THz and FIR spectroscopic measurements

Gretel M. Png,[1,*] **Bernd M. Fischer,**[2] **Dominique Appadoo,**[3] **Ruth Plathe,**[3] **and Derek Abbott**[1]

[1]*School of Electrical and Electronic Engineering, University of Adelaide, SA 5005, Australia*
[2]*French-German Research Institute of Saint-Louis, 68300 Saint-Louis, France*
[3]*The Australian Synchrotron, Clayton, VIC 3168, Australia*
[*]*gretel.png@adelaide.edu.au*

Abstract: In terahertz (THz) and far-infrared (FIR) spectroscopic measurements, weak absorption spectral features due to small quantities of test sample can be masked by undesirable etalon fringe artifacts caused by multiple reflections within a pellet or a rigid sample holder. A double-layered nitrocellulose (NC) membrane structure is proposed in this paper as an alternative holder for small quantities of either dry or wet pure (no added polyethylene powder) samples with significantly reduced etalon artifacts. Utilizing a THz time-domain spectroscopy system and a synchrotron source, we demonstrate the performance of the NC structure across the THz/FIR spectrum, benchmarking against pellets holding similarly small quantities of α-lactose powder either with or without different grades of polyethylene powder. With only pure samples to consider, scattering can be mitigated effectively in NC-derived spectra to reduce their baselines.

OCIS codes: (300.6495) Spectroscopy, terahertz; (300.6270) Spectroscopy, far infrared; (120.4290) Nondestructive testing; (290.5850) Scattering, particles; (000.2170) Equipment and techniques.

References and links

1. T. D. Dorney, R. G. Baraniuk, and D. M. Mittleman, "Material parameter estimation with terahertz time-domain spectroscopy," J. Opt. Soc. Am. A **18**(7), 1562–1571 (2001).
2. M. Kaushik, B. W.-H. Ng, B. M. Fischer, and D. Abbott, "Terahertz scattering by two phased media with optically soft scatterers," J. of Appl. Phys. **112**(11), 113112 (2012).
3. M. Kaushik, B. W.-H. Ng, B. M. Fischer, and D. Abbott, "Terahertz scattering by granular composite materials: An effective medium theory," Appl. Phys. Lett. **100**(1), 011107 (2012).
4. M. W. Nicholas and K. Nelson, "North, South, or East? Blotting Techniques," J. of Investigative Dermatology **133**(7), E1–E3 (2013).
5. M. N. Costa, B. Veigas, J. M. Jacob, D. S. Santos, J. Gomes, P. V. Baptista, R. Martins, J. Inacio, and E. Fortunato, "A low cost, safe, disposable, rapid and self-sustainable paper-based platform for diagnostic testing: lab-on-paper," Nanotechnology **25**(9), 094006 (2014).
6. Y. H. Tan, M. Liu, B. Nolting, J. G. Go, J. Gervay-Hague, and G. Liu, "A nanoengineering approach for investigation and regulation of protein immobilization," ACS Nano **2**(11), 2374–2384 (2008).
7. E. R. Tovey and B. A. Baldo, "Protein binding to nitrocellulose, nylon and PVDF membranes in immunoassays and electroblotting," J. Biochem. Biophys. Methods **19**(2–3), 169–183 (1989).
8. D. Grischkowsky, S. R. Keiding, M. van Exter, and C. Fattinger, "Far-infrared time-domain spectroscopy with terahertz beams of dielectrics and semiconductors," J. Opt. Soc. Am. **7**(10), 2006–2015 (1990).
9. M. van Exter, C. Fattinger, and D. Grischkowsky, "Terahertz time-domain spectroscopy of water vapor," Opt. Lett. **14**(20), 1128–1130 (1989).

#225002 - $15.00 USD Received 15 Oct 2014; revised 22 Dec 2014; accepted 4 Feb 2015; published 18 Feb 2015

10. X. Xin, H. Altan, A. Saint, D. Matten, and R. R. Alfano, "Terahertz absorption spectrum of *para* and *ortho* water vapors at different humidities at room temperature," J. Appl. Phys. **100**(9), 094905 (2006).
11. G. D. Dean and D. H. Martin, "Inter-molecular vibrations of crystalline polyethylene and long-chain paraffins," Chem. Phys. Lett. **1**(9), 415–416 (1967).
12. J. W. Fleming, G. W. Chantry, P. A. Turner, E. A. Nicol, H. A. Willis, and M. E. A. Cudby, "Temperature effects and observation of B_{2u} lattice mode in far infrared absorption spectrum of polyethylene," Chem. Phys. Lett. **17**(1), 84–85 (1972).
13. J. R. Birch, "The far infrared optical constants of polyethylene," Infrared Phys. **30**(2), 195–197 (1990).
14. P. F. Fox and P. L. H. McSweeney, *Dairy Chemistry and Biochemistry* (Blackie Academic & Professional, 1998).
15. J. L. Crisp, S. E. Dann, M. Edgar, and C. G. Blatchford, "The effect of particle size on the dehydration/rehydration behaviour of lactose," International J. Pharmaceutics **391**(1–2), 38–47 (2010).
16. B. T. Kurien and R. H. Scofield, "Protein blotting: A review," J. Immunological Methods **274**(1–2), 1–15 (2003).
17. G. M. Png, R. J. Falconer, B. M. Fischer, H. A. Zakaria, S. P. Mickan, A. P. J. Middelberg, and D. Abbott, "Terahertz spectroscopic differentiation of microstructures in protein gels," Opt. Express **17**(15), 13102–13115 (2009).
18. H. A. Zakaria, B. M. Fischer, A. P. Bradley, I. Jones, D. Abbott, A. P. J. Middelberg, and R. J. Falconer, "Low-frequency spectroscopic analysis of monomeric and fibrillar lysozyme," Appl. Spectrosc. **65**(3), 260–264 (2011).
19. K. Shiraga, Y. Ogawa, N. Kondo, A. Irisawa, and M. Imamura, "Evaluation of the hydration state of saccharides using terahertz time-domain attenuated total reflection spectroscopy," Food Chemistry **140**(1–2), 315–320 (2013).
20. Y. Listiohadi, J. A. Hourigan, R. W. Sleigh, and R. J. Steele, "Moisture sorption, compressibility and caking of lactose polymorphs," International J. Pharmaceutics **359**(1–2), 123–134 (2008).
21. J. H. Kirk, S. E. Dann, and C. G. Blatchford, "Lactose: A definitive guide to polymorph determination," International J. Pharmaceutics **334**(1–2), 103–114 (2007).
22. R. Lefort, V. Caron, J.-F. Willart, and M. Descamps, "Mutarotational kinetics and glass transition of lactose," Solid State Communications **140**(7–8), 329–334 (2006).
23. M. Hineno and H. Yoshinaga, "Far-infrared spectra of galactose and lactose at liquid He temperature," Spectrochimica Acta Part A: Molecular and Biomolecular Spectroscopy **A29**(2), 301–305 (1973).
24. C. F. Bohren and D. R. Huffman, *Absorption and Scattering of Light by Small Particles*, (John Wiley & Sons, 1983).
25. H. Vromans, A. H. De Boer, G. K. Bolhuis, C. F. Lerk, K. D. Kussendrager, and H. Bosch, "Studies on tableting properties of lactose. Part 2: Consolidation and compaction of different types of crystalline lactose," Pharmaceutisch Weekblad-Scientific Edition **7**(5), 186–193 (1985).
26. V. Busignies, P. Tchoreloff, B. Leclerc, M. Besnard, and G. Couarraze, "Compaction of crystallographic forms of pharmaceutical granular lactoses. I. Compressibility," Eur. J. Pharm. Biopharm. **58**(3), 569–576 (2004).
27. M. Franz, B. M. Fischer, and M. Walther, "The Christiansen effect in terahertz time-domain spectra of coarse-grained powders," Appl. Phys. Lett. **92**(2), 021107 (2008).

1. Introduction

A common technique for performing spectroscopic measurements of powdered samples in the far-infrared (FIR) or terahertz (THz) frequency range is to combine the sample with a bulking/binding medium such as polyethylene (PE) powder, pressing the mixture into a pellet (of the order of 10 mm in diameter), and then placing the pellet in the path of the radiation. This technique is simple and well-established, but it does have several limitations with regards to sample quantity and artifacts.

A pellet needs to be mechanically robust in order to be removed from the pellet die and mounted on a sample holder. When very small quantities of samples are available (e.g.$<$ 50 mg of α-lactose), there is insufficient sample to make a robust $\approx$10 mm pellet so polyethylene (PE) powder needs to be added as a bulking material. Alternatively, pellets with smaller diameters can be pressed in order to reduce the amount of bulking material used, however the beam waist of the incident radiation should ideally be equal or narrower than the small pellet's surface area in order to maximize the benefit.

If the beam waist is broader than the diameter of the pellet, then the beam will be clipped by the sample holder and be attenuated, resulting in a reduction the amplitude of the measured signal as shown in Fig. 1(a). The reduction in signal amplitude leads to a reduction in the signal-to-noise ratio (SNR) of the experiment, which is undesirable especially in instances when only

#225002 - $15.00 USD Received 15 Oct 2014; revised 22 Dec 2014; accepted 4 Feb 2015; published 18 Feb 2015

a very small quantity of sample is available for measurement.

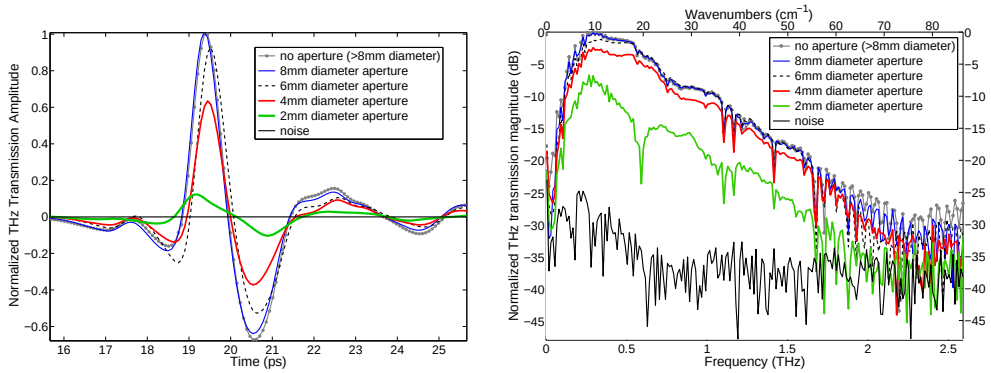

(a) Reduction in the SNR with decreasing aperture size

(b) Corresponding reduction in the dynamic range

Fig. 1. Transmission-mode measurements using a Menlo Tera K15 THz time-domain spectroscopy (TDS) system, utilizing photoconductive antennas to generate and detect THz radiation. More details of the Menlo Tera K15 system are provided in Section 3.1. (a) Keeping the beam waist of the incident radiation constant, the measured signal amplitude falls as the diameter of the focal point reduces, resulting in a poorer SNR. The maximum signal amplitude (no aperture present) is normalized to one. The noise measurement is made by blocking off the THz radiation; (b) Normalized frequency responses of the plots in Fig. 1(a) show the decreasing dynamic range with decreasing aperture size.

Figure 2 shows the spectral information obtained from small quantities of α-lactose monohydrate (Sigma L3625) mixed with 50 mg of PE (Aldrich 434272), pressed as pellets (each with 13 mm diameter) under 10 tonnes of pressure for 15 minutes. This quantity of PE is used as we find that it is the minimum amount for our test pellets to be pressed, handled and measured without crumbling. Mixing a sample with PE means that the sample is distributed over the volume of a pellet; the sample is effectively "diluted" by the PE, resulting in a deterioration of the spectral signature as the sample quantity is reduced. Additionally, we test the scenario where 6 mg of α-lactose is purposely placed in the center of the pellet to increase the likelihood of interaction between α-lactose and the THz beam, but this does not improve the quality of the measured signal.

One artifact that is inextricable with the use of pellets is the Fabry-Pérot etalon effect in a slab. This artifact is of particular concern for optically thin pellets. In THz time-domain spectroscopic (THz-TDS) experiments, time-gating is employed to capture the transmitted signal from a sample, but this technique inadvertently captures reflections from the body of the pellet that emerge after the main signal pulse has transmitted through the sample [1]. The resulting artifact, which manifests as oscillations in the baseline of the spectrum as seen for the 4 mg and 6 mg scenario in Fig. 2, can be reduced through signal processing of the data (e.g. filtering). For the 2 mg scenario, the oscillations dominate the spectrum, making it difficult to recover the weak sample spectrum.

Another artifact present in pellets is scattering from the PE bulking medium and the powdered sample, manifesting as a rise in the baseline of the spectrum that can be mitigated through additional signal processing that requires *a priori* knowledge of the size of the scatterers [2]. The use of PE with the smaller granular size can help reduce scattering [3], but as shown in Fig. 3(a), the use of PE with smaller granular size (average diameter of 50–70 μm, Inducos 13/1 from Induchem AG, Switzerland) does not reduce scattering in our case. Furthermore, as shown

#225002 - $15.00 USD Received 15 Oct 2014; revised 22 Dec 2014; accepted 4 Feb 2015; published 18 Feb 2015

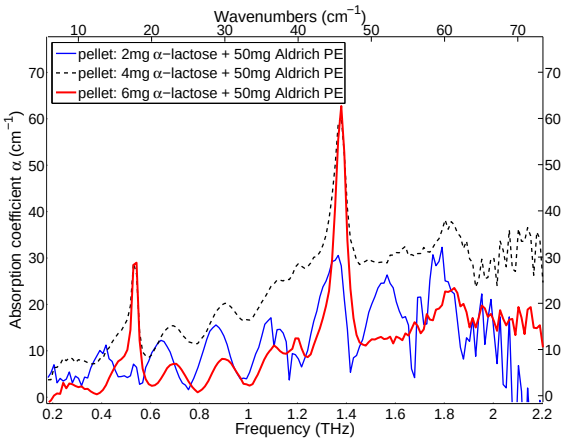

Fig. 2. A comparison of the room temperature absorption coefficients of small quantities of α-lactose monohydrate mixed with 50 mg of PE and pressed into 13 mm pellets, measured with a Menlo THz-TDS system. The spectral peaks in this frequency range are at 0.54 THz, 1.2 THz, 1.38 THz and 1.83 THz (18 cm^{-1}, 40 cm^{-1}, 46 cm^{-1} and 61 cm^{-1} wavenumbers respectively). The oscillatory artifact from the Fabry-Pérot etalon effect strongly masks the spectral signature for the 2 mg scenario. No useful data is obtained for a 1 mg scenario.

in Fig. 3(b), the finer-grain PE did not enhance the spectral features for the small quantity of α-lactose.

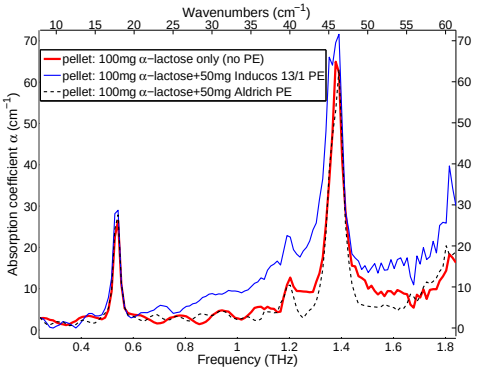

(a) Absorption profiles of pure and mixed pellets, each containing a large quantity of α-lactose

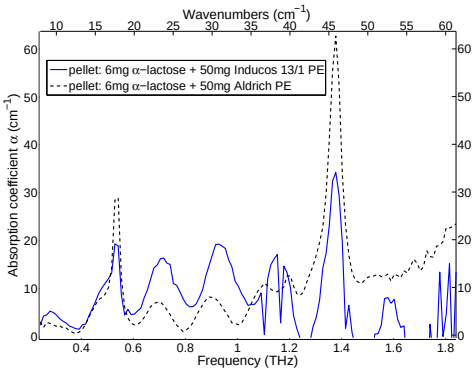

(b) Absorption profiles of mixed pellets, each containing a small quantity of α-lactose

Fig. 3. (a) A comparison of the room temperature absorption coefficients (measured with a Menlo THz-TDS system) of 100 mg α-lactose powder when pressed into a pellet consisting of (i) pure α-lactose (thick red line), (ii) mixed with 50 mg Inducos 13/1 PE with average granular diameter of 50–70 μm (blue line), and (iii) mixed with 50 mg Aldrich PE with average granular diameter of 72 μm (dashed black line); (b) When a very small quantity of sample is present in a pellet, the use of PE with smaller granular size (Inducos 13/1, 50–70 μm average diameter) as a bulking material does not enhance the spectral features of the sample.

The ability to detect a small quantity of sample in the THz frequency range has immense value in clinical applications where only minute quantities (micrograms up to milligrams) of bi-

#225002 - $15.00 USD Received 15 Oct 2014; revised 22 Dec 2014; accepted 4 Feb 2015; published 18 Feb 2015

ological markers can be realistically extracted from body fluids. The sensitivity of a laboratory-based THz system can be improved through high-quality optical components and careful tuning, but a limit will eventually be reached after which novel sample holders, such as microfluidic cells and waveguides, may be required to further enhance the detection sensitivity. However, these latter holders can be expensive to fabricate. In this paper, we introduce a novel, effective and comparatively cost-efficient technique involving the use of nitrocellulose membranes for holding both dry and wet samples without the use of bulking materials, significantly reducing the problems associated with etalon effects without additional signal processing of the data.

2. Nitrocellulose membranes

Nitrocellulose (NC) membranes are a type of transfer medium used routinely to bind proteins in immunoblot techniques, such as Western, Northern and Southern blots [4]. Other types of transfer membranes exist (e.g. cellulose, polyvinylidene or PVDF) but NC was chosen for our study as it does not require pre-wetting when compared to PVDF, and it has a low degree of crystallinity when compared to cellulose [5]. As shown in Fig. 4, NC contains a network of fibers that creates the NC's micropore structure, with a rough surface that allows proteins to bind instantaneously to it. The pore size determines the binding capacity of NC.

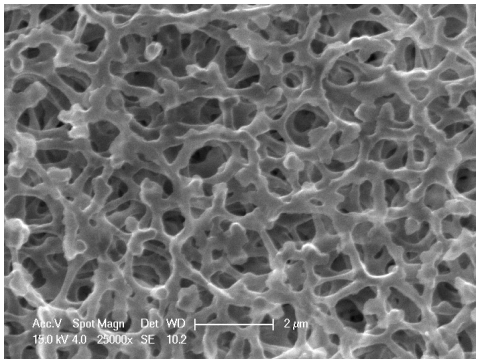

Fig. 4. Scanning electron microscope (SEM) micrograph of a layer of nitrocellulose membrane with 0.2 μm pore size, showing the network of fibers that creates the NC's micropore structure. The white scale bar represents 2 μm.

In this study, we use two types of NC from GE Healthcare's Amersham Protran range (formerly Whatman Protran). The types of NC are: 10600000 (formerly BA79) with 0.1 μm pore size and 10600001 (formerly BA83) with 0.2 μm pore size. As reported by the manufacturer, the protein binding capacity for NC with 0.1 μm pore size is 231–248 μg·IgG/cm^2, which is suitable for particles with molecular weight $<$ 10 kDa. The protein binding capacity for NC with 0.2 μm pore size is 150–176 μg·IgG/cm^2, which is suitable for particles with molecular weight $<$ 20 kDa. To put in perspective the structure of NC in terms of physical size, an immunoglobin G (IgG) molecule is approximately 10 nm in diameter [6] and has molecular weight of 150 kDa. At 160 μg·IgG/cm^2 binding capacity, 6.4255×10^{14} molecules of IgG will bind to the fibers in 1 cm^2 of NC with a 0.2 μm pore size. The pores in the NC allow for the movement of fluid in situations where proteins are suspended in solution. The protein binding capacity improves with smaller pore size as there is more surface area for protein binding. More information about protein binding on membranes can be found in [7].

#225002 - $15.00 USD Received 15 Oct 2014; revised 22 Dec 2014; accepted 4 Feb 2015; published 18 Feb 2015

3. Comparison of the optical properties of NC and PE

In this study, we use two sources of THz in order to study NC over a wide frequency range (0.2–19 THz). The next sub-section describes the instruments used in our experiments. The subsequent sub-section presents results from our experiments.

3.1. Instruments for experiments

For experiments conducted in the lower THz frequency range ($\leq$ 2 THz), we utilize a Menlo Tera K15 modular THz time-domain spectroscopy (THz-TDS) system operating in transmission-mode. The Menlo Tera K15 contains an erbium-doped silica fiber laser source that generates femtosecond pulses, each with width of $<$ 90 fs and 1560 nm center wavelength. The laser is first fiber-coupled to an optical light path with a delay line, and then fiber-coupled to the THz emitter and detector modules. A stripline InGaAs/InAlAs photoconductive antenna (PCA) is used for THz emission, and a dipole LT (low-temperature grown) InGaAs/InAlAs PCA antenna is used for detection. The collimated beam from the THz emitter has a diameter of 20 mm; 1.5" (38 mm) TPX polymer lenses are used to focus the beam down to 8 mm at the focal point. The SNR as shown in Fig. 1(b) is -25 dB. The lock-in amplifier's integration time-constant is set at 100 ms. Each recorded data set is averaged over three scans. Each plot presented in this paper is averaged over three recorded data sets (i.e. nine scans).

For experiments conducted in the higher THz frequency range ($>$ 2 THz), we utilize a Fourier Transform InfraRed (FTIR) spectrometer (Bruker IFS 125/HR) with a synchrotron radiation source (Australian Synchrotron, Clayton VIC) in conjunction with a 6 μm multilayer mylar beamsplitter. Measurements are made at 77 K under vacuum using a liquid nitrogen-cooled cryostat (Janis Research). Signals are detected with a liquid helium-cooled Si bolometer. Each recorded data set is averaged over 100 scans; we record five data sets per sample. The beam waist of the incident THz radiation at the focal point is under 3 mm, allowing the use 3 mm pellets that were previously unsuitable in the THz-TDS system with an 8 mm beam waist. Additionally, the reliable bandwidth of the FTIR system with no sample present is from 2–21 THz but we have found it is possible to extend the bandwidth down to 1.5 THz for some of our measurements. As shown later in Figs. 7 and 11, the upper limit of the reliable bandwidth decreases with the types of samples measured.

The NC membranes have thicknesses of 95 μm (0.2 μm pore size) and 100 μm (0.1 μm pore size), making them paper-like. In order to hold the NC upright in the path of the THz radiation, we mount the NC on a metal washer with an inner diameter that is wider than the beam waist at the focal point. This washer is then placed at the THz focal point. To achieve a double-layered NC structure that is referred to later in Section 4, we find that sandwiching two washer-mounted NC is easier than placing one unmounted NC membrane on top of another because the NC membranes are electrostatic and will repel. Figure 5 illustrates a multi-sample holder that we designed to facilitate sample loading and sandwiching for the Synchrotron measurements. The sample holders are made of 0.32 mm thick copper to allow for good thermal conductivity at low measurement temperatures under vacuum while maintaining mechanical strength.

In the following sections, plots of the THz absorption properties of the samples are presented. Calculations for the THz absorption coefficient require knowledge of the thicknesses of the samples. We measure the thickness of the washers before and after loading a sample, utilizing the difference to obtain the sample's thickness.

3.2. Experiments

Figure 6(a) presents a comparison of the THz absorption properties α and refractive indices n of NC and PE. Although α_{NC} is not as flat as that of α_{PE}, it is still excellent as there is only a gradual rise across the frequency range from 0.2 to $\approx$1.8 THz, with no obstructive spectral

#225002 - $15.00 USD Received 15 Oct 2014; revised 22 Dec 2014; accepted 4 Feb 2015; published 18 Feb 2015

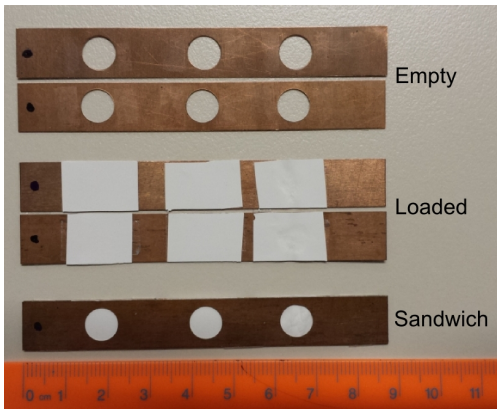

Fig. 5. Three views of the copper sample holder designed to facilitate the loading of samples and sandwiching to create the double-layered NC structure. (Top) empty holder; (middle) loaded with NC; (bottom) sandwich structure. This sample holder is used for measurements made at the Australian Synchrotron at 77 K under vacuum.

peaks or etalon artifacts. The profile and magnitude of α_{NC} is reminiscent of that of fused silica (amorphous quartz glass) [8].

The rise in α_{NC} is expected to plateau at $\alpha \approx 12$ cm^{-1} for the 0.2 μm pore size and $\alpha \approx 19$ cm^{-1} for the 0.1 μm pore size; a verification of this observation is presented in the next paragraph. The difference between α_{NC} for the two types of NC is expected as NC with 0.1 μm pore size is denser than NC with 0.2 μm pore size. This is also reflected in the refractive index of the two types of NC as shown in Fig. 6(b), where the 0.1 μm pore size NC has a slightly higher refractive index. Similar to PE, the n_{NC} profiles for both types of NC are flat across the 0.2 to $\approx$1.8 THz range.

To confirm that the NC's optical properties are comparable to that of PE at higher THz frequencies, we measure PE and NC using a FTIR spectrometer as described in Section 3.1. A comparison of absorption properties of PE and NC at frequencies above 2 THz is presented in Fig. 7. We have included the measurement of NC from another manufacturer (Pall BioTrace NT, 0.2 μm pore size) to ascertain if the optical properties of NC reported in this paper is manufacturer-dependent; a discussion of our findings is presented next.

There are three notable observation from Fig. 7. Firstly, α_{NC} of all three NC samples do indeed plateau until around 4 THz, after which α_{NC} rises to a little below $\alpha = 120$ cm^{-1}. Secondly, the plots of the all three NC samples have very similar absorption profiles, with only slight offsets between plots. We have further measured these samples on another FTIR spectrometer with a mercury-arc lamp THz source (Bruker Vertex 70v, results not shown) and have obtained similar findings, hence the differences in THz absorption is most likely due to differences in densities between the three samples as mentioned earlier in this sub-section, with the 0.1 μm sample being the densest hence most absorbing. The two 0.2 μm samples are not truly identical as there are physical differences between them, which may attribute to the dissimilarity in their THz absorption. Nonetheless, the THz absorption profiles of all three samples are very similar, which indicates that the THz absorption property of NC is nearly consistent across different manufacturers. Henceforth, due to product availability, our study is based on NC from GE Healthcare's Amersham Protran range.

The third observation from Fig. 7 is that α_{PE} from Aldrich differs significantly from that of Inducos 13/1 in that there is a pronounced rise in α_{PE} for Aldrich PE, and that there are two spectral peaks at $\approx$3.2 THz (107 cm^{-1} wavenumbers) and $\approx$7.2 THz (240 cm^{-1} wavenumbers)

#225002 - $15.00 USD Received 15 Oct 2014; revised 22 Dec 2014; accepted 4 Feb 2015; published 18 Feb 2015

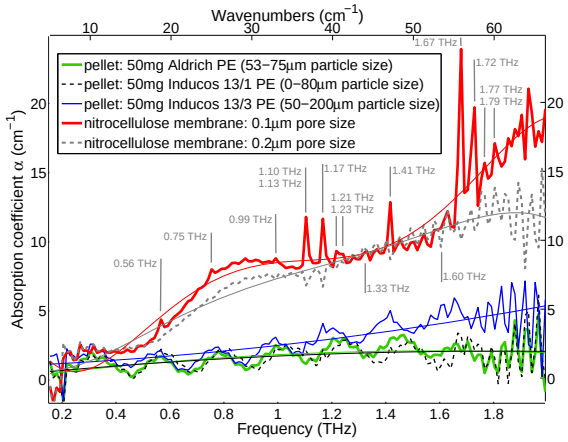

(a) Absorption profiles of PE pellets (three different grain sizes) and two types of NC. Spectral locations of the water vapor lines as reported in [9, 10] are annotated with gray lines and text.

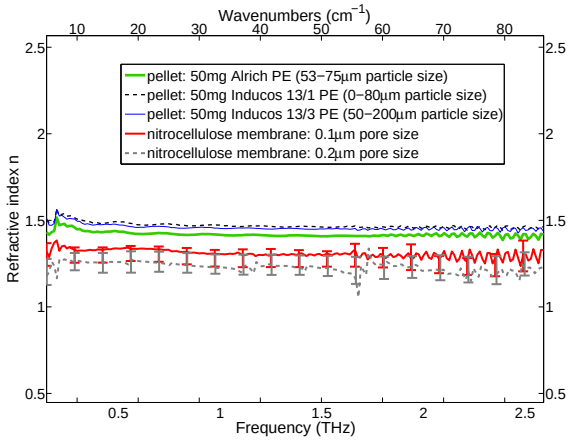

(b) Refractive index profiles of the various PE and NC samples

Fig. 6. (a) Absorption coefficients α of various double-layered NC structures and PE from 0.2–1.8 THz at 298 K, measured with a THz-TDS system. The peaks in α_{NC} are due to residual water vapor lines. The overall α_{NC} profiles are smooth as shown by the fitted curves. Although α_{NC} is not as flat and low as α_{PE}, it still possesses good THz transmissivity with no etalon artifacts; (b) Refractive indices n of various double-layered NC structures and PE from 0.2–1.8 THz at 298 K. Like n_{PE}, the n_{NC} profiles are flat across the frequency of interest. The peaks along n_{NC} correspond to water vapor lines.

as indicated by the arrows. We note that $\alpha_{PE} < 0$ below 4 THz for both PE samples, implying that the α_{PE} values are unreliable in this frequency range but the spectral peak at $\approx$3.2 THz is indeed genuine as reported in [11–13]; the two peaks are due to PE from Aldrich having a long polymeric structure typical for ultra-high molecular weight PE (UHMWPE). Conversely, PE from Inducos is high density PE (HDPE) that has a short polymeric structure with less distinct spectral peaks. Unlike the three NC samples that have similar THz optical properties across the frequencies of interest, the two PE samples have starkly different optical properties at higher frequencies, highlighting the variability in PE across manufacturers. Comparing the NC and PE plots, the absorption property of NC lies between those of UHMWPE (Aldrich) and HDPE

#225002 - $15.00 USD Received 15 Oct 2014; revised 22 Dec 2014; accepted 4 Feb 2015; published 18 Feb 2015

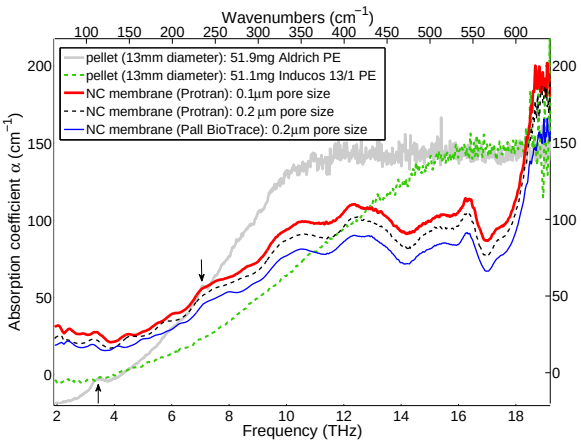

Fig. 7. Absorption coefficients α of various NC and PE samples from 1.5–19 THz at 77 K, measured with a synchrotron THz source. Here, α_{PE} of both types of PE are lower than α_{NC} at lower frequencies but rise significantly at higher frequencies, with α_{PE} of the Aldrich PE surpassing α_{NC} from 7 THz onwards. The spectral peaks of PE at ≈3.2 THz and ≈7.2 THz are consistent with that in literature [11–13].

(Inducos), hence it is a viable candidate as a sample holding medium as will be demonstrated in the next section.

4. Performance benchmarking and discussion

We use α-lactose monohydrate (Sigma L3625, molecular weight 360 Da) to benchmark the performance of NC because the THz spectral signature of α-lactose is well characterized. Depending on the grade of α-lactose (e.g. research, pharmaceutical, edible), each tomahawk-shaped crystal can be between 1 μm up to several hundred microns in length [14, 15]; this is many times larger than the pore size of NC as shown in Fig. 8. This figure shows crystals with assorted lengths (≈20 μm on average) of research-grade α-lactose that is used in this work.

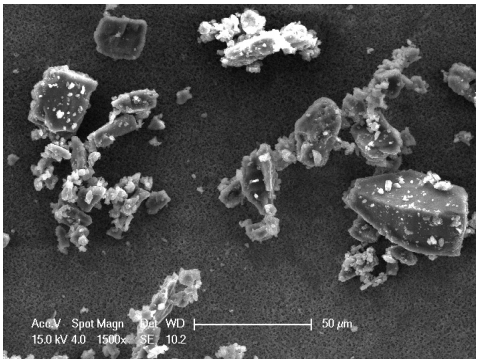

Fig. 8. SEM micrograph of dry α-lactose powder on a layer of NC with 0.2 μm pore size. The white scale bar represents 50 μm.

Some α-lactose crystals will bind weakly to the rough surface of the NC but can fall off easily when disturbed by movement or air flow. Consequently, we find that sandwiching the α-lactose between two layers of NC provides a means of holding larger quantities of sample

#225002 - $15.00 USD Received 15 Oct 2014; revised 22 Dec 2014; accepted 4 Feb 2015; published 18 Feb 2015

without sacrificing THz transmissivity. A multilayer structure can be used to hold even more sample but then we begin to observe weak oscillations in the spectra that indicate the presence of etalon effects, therefore the double-layered structure introduced in Section 3.1 has the least artifacts while providing good sample holding capacity.

Another benefit of NC worth noting is that it is used in immunoblot applications that involve immobilizing proteins that exist in a gel [16]. The measurement of aqueous samples is a challenge in THz transmission-mode experiments because of the strong attenuation by water. Freezing [17], gelation and lyophilization [18] are techniques used previously by other authors to either remove water or alter the physical state of water. Attenuated total reflection THz spectroscopy is an alternative to transmission-mode measurements and it has been applied to the study of hydration states in saccharides, but the high water content quenches the intermolecular vibration modes that produce the distinct spectral peaks of saccharides [19].

In this study, the α-lactose samples measured at the Australian Synchrotron are mixed with 10–20 μl of MilliQ water and applied directly onto the NC with a pipette—a technique akin to loading a sample in dot blotting. Figure 9 shows an α-lactose crystal on the NC after being loaded using the pipette loading technique. This crystal has caked as a result of the hydration [20]. Although the sample is left to air dry prior to measurement to reduce the influence from water on the THz measurement, we were concerned with two issues: the effect of caking, and the possibility of mutarotation of the α-lactose molecules due to the presence of water [21,22]. As will be seen later in Table 1, the results from our measurements strongly show that caking has not altered the α-lactose molecules and that mutarotation, which is the interconversion between α-lactose and β-lactose anomers in a solution, has not occurred.

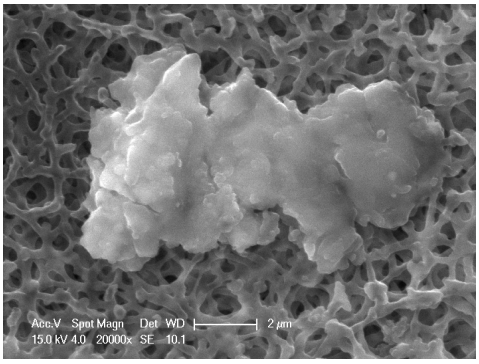

Fig. 9. SEM micrograph of damp α-lactose crystal on a layer of NC with 0.2 μm pore size. This crystal has caked as a result of hydration. The white scale bar represents 2 μm.

We note here that the α-lactose samples measured using the THz-TDS system were completely dry. The THz peak power from a synchrotron source is several orders stronger (hundreds of watts) than from a TDS system (tens of milliwatts). The presence of water, with its known strong THz absorption property, is a formidable obstacle for TDS experiments. Despite drying the samples for a longer duration than when using the synchrotron source, we did not obtain any meaningful data from these pre-wetted samples hence only dry samples were used. Conversely, only measurements of pre-wetted samples made at the Synchrotron are presented in this work because of the challenges encountered with pre-wetted samples for a TDS system.

4.1. Results

Laboratory (TDS) and synchrotron (FTIR) measurements are shown in Figs. 10 and 11. As mentioned in Section 3.1, the narrow beam waist of the incident THz radiation at the Aus-

#225002 - $15.00 USD Received 15 Oct 2014; revised 22 Dec 2014; accepted 4 Feb 2015; published 18 Feb 2015

tralian Synchrotron enables us to use pellets with 3 mm diameter, hence we are able to press a pellet containing 6 mg of pure α-lactose in order to eliminate the influence of PE on measurements. The spectral features extracted from this 3 mm pellet are presented in Fig. 11(a) and is the standard upon which we benchmark the NC's performance at higher THz frequencies. Additionally, we have included the absorption profile of 8 mg of α-lactose in NC at room temperature in order to investigate the performance of the NC holder at a higher test temperature. At lower THz frequencies where a TDS system is used for measurements, we utilize a 13 mm pellet containing 80 mg of pure α-lactose as the standard; this amount of α-lactose was the minimum quantity that permitted the making of a robust pellet that did not crumble when handling.

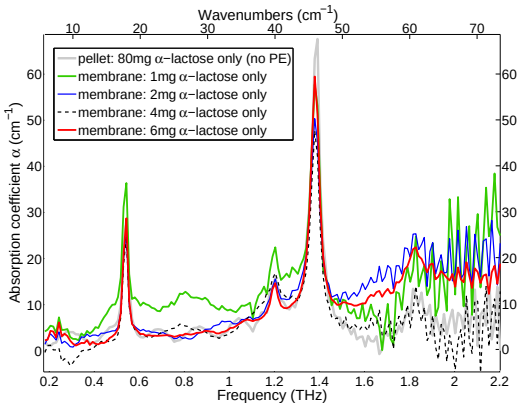

(a) Room temperature absorption coefficients of α-lactose as a pure pellet and in the double-layered NC holder, measured from 0.2–2.2 THz with a THz-TDS system.

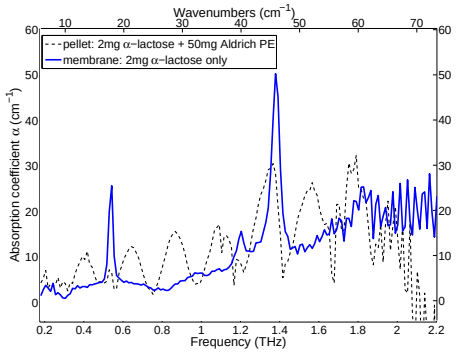

(b) A comparison of the pellet-held 2 mg sample from Fig.2 and the NC-held 2 mg sample from Fig. 10(a), showing significantly less etalon artifacts from the NC holding medium.

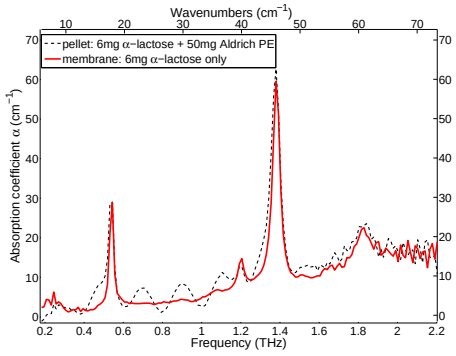

(c) A comparison of the pellet-held 6 mg sample from Fig.2 and the NC-held 6 mg sample from Fig. 10(a). The peak at 1.83 THz is discernible for both samples but is more distinct for the NC-held sample.

Fig. 10. Compared to the pure pellet, there is significantly less masking by etalon artifacts in the NC-held samples, resulting in the clear revelation of the smaller spectral peak at 1.2 THz, particularly for the 2 mg NC-held sample. No signal processing has been applied to enhance these plots.

Comparing Figs. 2 and 10, the notable advantage of using the NC holder is the significant reduction of etalon artifacts, resulting in the clear revelation of the small peak at 1.2 THz for all quantities of α-lactose in NC. The next small peak at 1.83 THz is near to the noise floor

#225002 - $15.00 USD Received 15 Oct 2014; revised 22 Dec 2014; accepted 4 Feb 2015; published 18 Feb 2015

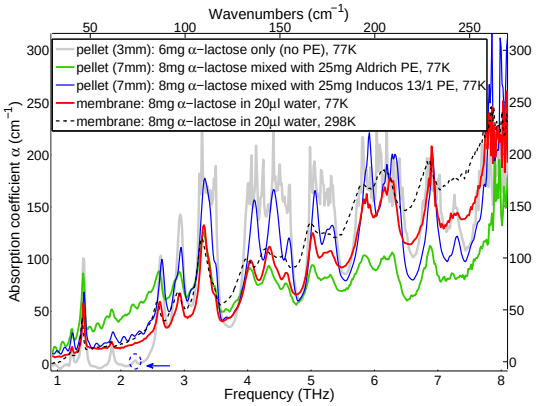

(a) High frequency absorption profiles of α-lactose as pellets and in the double-layered NC holder

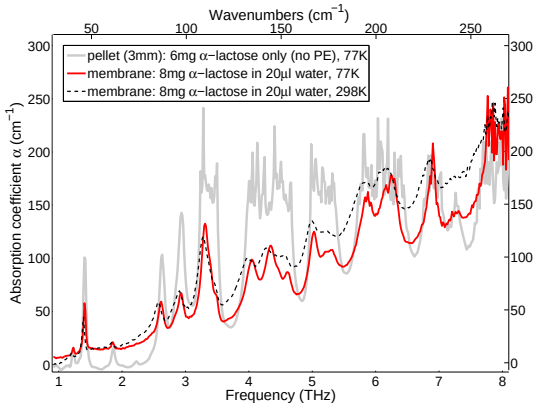

(b) Extract from Fig. 11(a) showing only the NC-held samples and the pure pellet

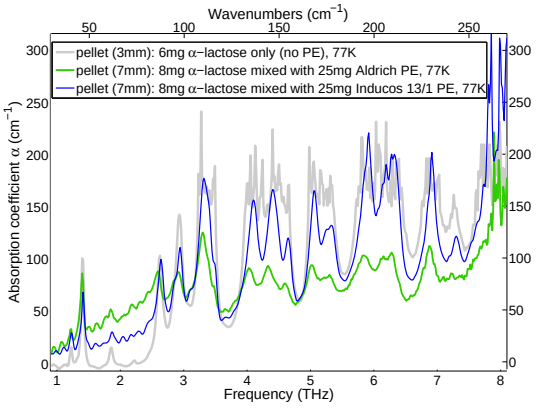

(c) Extract from Fig. 11(a) showing only the mixed pellets and the pure pellet

Fig. 11. (a) Absorption coefficients from 0.6–8.1 THz at 77 K and 298 K, measured with a synchrotron THz source. The circle highlights the weak peak at 2.21 THz that is most visible for the pure pellet; (b) There is excellent overlap of the troughs from the 77 K NC-held sample and the 3 mm pure pellet, with similar rising baselines that is likely due to scattering by the α-lactose crystals. The peaks of the 298 K NC-held sample are red shifted; (c) The etalon artifacts are most prominent at low frequencies for both mixed pellets. The rise in baseline for the pellet containing Aldrich PE is very distinct from that of the other two samples.

#225002 - $15.00 USD Received 15 Oct 2014; revised 22 Dec 2014; accepted 4 Feb 2015; published 18 Feb 2015

of this THz system thus is less distinct, even for the pure 80 mg pellet. However this peak is discernible for all samples in NC, particularly for the 6 mg sample. This peak is also discernible in Figs. 2 and 10(c) for the PE-held 6 mg sample but is less distinct when compared to the peak of the NC-held 6 mg sample.

Referring to Fig. 11(a) for the higher frequency measurements, there are three observations that are interesting. Firstly, the spectral peaks of the 3 mm pure α-lactose pellet are attenuated from 3 THz onwards as they exceed the maximum detectable absorption (i.e. saturated), however the spectral troughs are well-defined. Although we do not have peak absorption intensity values to compare against those obtained from the other samples, we can use the spectral positions and absorption coefficients of the troughs as a comparison. Secondly, unlike in the low frequency range as shown in Fig. 3(b), the use of Inducos 13/1 PE does indeed improve the detection of spectral features in the sample. Thirdly, as expected, the quality of the peaks of the 77 K NC-held sample falls between those of HDPE and UHMWPE, but has the advantage of not containing etalon artifacts at lower frequencies.

4.2. Spectral location of peaks and troughs

In terms of spectral position of the troughs, there is excellent agreement from ≈3–5.5 THz between all four samples measured at 77 K. In terms of absorption coefficient values of the troughs, there is agreement above ≈2.8 THz between the pure pellet, the 77 K NC-held sample and the 7 mm pellet containing Inducos 13/1 PE; additionally all three samples have similar rising baselines towards higher frequencies. As expected, the peaks of the 298 K NC-held sample are shifted towards lower frequencies (red shift) due to the higher test temperature.

The 7 mm pellet containing Aldrich PE has a particularly steep rising baseline until ≈3 THz as seen in Fig. 11(c), whereby the gradient of this baseline differs from those of the other three samples made at 77 K. Above 3.5 THz, the baseline of this 7 mm pellet flattens out more than the baselines of the other samples. The differences between the two 7 mm pellets are *(i)* the size of the PE grains and *(ii)* the type of PE (UHMWPE and HDPE). Since the baseline of the pellet containing Inducos 13/1 PE is similar to those of the three samples without PE, then it is likely that scattering from the α-lactose crystals is the cause of the rising baseline in these four samples, whereas scattering from the larger PE grains is the likely cause of the steep rise in baseline for the 7 mm pellet containing Aldrich PE—this will be verified in the next section.

The locations of the spectral peaks of all samples mostly agree with those reported in [23], where anhydrous lactose (containing both the α-lactose and β-lactose anomers) is measured at 4 K and 298 K while suspended in mineral oil (Nujol). The absorption bands from [23] and this study are tabulated in Table 1. As highlighted above, the spectral peaks of samples measured at 298 K are shifted towards lower frequencies (red shift) due to the higher test temperature.

As discussed previously in Section 4, caking and mutarotation of the α-lactose crystals were of concern due to the presence of water of the samples that are loaded onto the NC. As seen in Table 1, the peaks extracted from the NC-held samples agree with those from the PE-held samples. Furthermore, the two additional peaks reported in [23] are likely due to the β-lactose anomers in anhydrous lactose, but these two peaks are not observed for the NC-held samples. This strongly indicates that mutarotation has not occurred in our NC-held samples, possibly due to very small quantity of water involved. Furthermore, the caking effect has not altered the α-lactose molecules. These two observations are very encouraging as they open up an avenue for using a synchrotron THz source for measuring aqueous samples without a liquid cell.

4.3. Scattering mitigation

To verify and remove the effect of scattering from the α-lactose crystals, we utilize the standard Mie scattering equations for spheres [24] to generate the scattering cross-section C_{sca} per unit

#225002 - $15.00 USD Received 15 Oct 2014; revised 22 Dec 2014; accepted 4 Feb 2015; published 18 Feb 2015

Table 1. Wavenumbers of the spectral peaks of anhydrous lactose at 4 K and 298 K [23], and α-lactose monohydrate at 77 K and 298 K (this work with a synchrotron THz source). The letter symbols in parentheses indicate the relative absorption intensity: s = strong, m = medium, w = weak, w? = very weak/doubtful. The X symbol indicates band not reported or not observed; the — symbol indicates no data available (signal exceeds either minimum or maximum detection limits). Ald. = Aldrich, Ind. = Inducos 13/1. The peaks shift toward lower wavenumbers (red shift) at higher measurement temperatures. Anhydrous lactose contains both α-lactose and β-lactose anomers thus may contain more bands (e.g. 83.5 cm^{-1} and 215 cm^{-1} wavenumbers) than those obtained in this study where $\geq$96% α-lactose anomers are present. On line 17 ($\approx$209 cm^{-1} wavenumbers) for the samples tested in this work, the cluster of peaks are likely to be from one strong, broad peak that has exceeded the maximum detection limit, splintering into several smaller but distinct peaks.

[23] oil mull (298 K)	**[23] oil mull (4 K)**	**6 mg pellet (77 K)**	**8 mg+Ald. PE pellet (77 K)**	**8 mg+Ind. PE pellet (77 K)**	**8 mg in NC (77 K)**	**8 mg in NC (298 K)**
—	—	40.5(m)	40.5(m)	40.5(m)	40.5(m)	39.5(m)
45.7(s)	47.2(s)	46.3(s)	46.3(s)	46.8(s)	46.3(s)	45.8(s)
X	62.1(w)	61.2(m)	61.2(m)	61.7(m)	61.2(m)	60.8(m)
X	75.5(w)	73.8(w)	72.3 etalon?	72.0 etalon?	73.8(w?)	X
X	83.5(m)	X	X	X	X	X
85.4(w)	89.3(s)	87.3(s)	86.3(s)	87.8(s)	86.8(s)	85.3(s)
96.4(w)	96.0(m)	94.0(w?)	94.5(w?)	95.0(w?)	94.0(w?)	X
	98.8(m)	97.4(s)	96.9(s)	97.9(s)	97.4(s)	96.4(s)
X	104(m)	X	103.0(w?)	103.0(w?)	102.5(w?)	X
109(s)	112(s)	—	109.9(s)	110.4(s)	109.9(s)	109.0(s)
X	117(m)	—	115.7(w)	115.5(w)	115.7(w)	114.8(w?)
132(m)	140(m)	—	134.0(s)	136.5(s)	134.5(s)	132.6(s)
143(m)	150(m)	—	144.1(s)	146.6(s)	144.6(s)	142.7(s)
152(m)	157(m)	—	152.8(m)	154.8(s)	153.3(m)	151.4(m)
167(m)	170(m)	—	166.8(s)	168.5(s)	167.3(s)	166.3(s)
		—	173.6(w?)	175(w?)	173.5(w?)	174.6(w?)
X	180(m)	—	176.5(w)	177.4(m)	176.9(m)	176.0(w?)
192(m)	198(m)	—	194.3(s)	197.2(s)	195.7(s)	194.3(s)
		—	204.9(w)	205.0(w)	205.4(w?)	204.9(s)
206(m)	209(m)	—	206.4(w?)	206.3(s)	206.4(s)	X
		—	209.2(s)	209.3(w?)	208.3(s)	X
		—		210.7(w?)	209.7(w)	X
X	215(m)	X	X	X	X	X
230(w)	232(m)	—	229.0(s)	230.5(s)	229.0(s)	228.3(s)
X	245(m)	—	240.6(w?)	243.5(m)	241.1(m)	—
262(m)	263(m)	—	—	—	—	—

volume of the α-lactose crystals. Crystalline α-lactose monohydrate is reported as being less susceptible to fragmentation under compaction than other lactose polymorphs [25,26], allowing the utilization of its known dimensions in our spherical model.

In the Mie scattering model, the standard THz absorption coefficient profile is treated as being the sum of scattering and absorption, known collectively as extinction. By calculating the

#225002 - $15.00 USD Received 15 Oct 2014; revised 22 Dec 2014; accepted 4 Feb 2015; published 18 Feb 2015

Mie scattering component (C_{sca} per unit volume), we can then subtract it from the measured extinction component to retrieve the scattering-mitigated absorption. The Mie model is a good approximation for our work across the 1–8 THz range, beyond which we exceed the usable bandwidth of the measurements, and the measured data becomes noisy.

The value of C_{sca} needs to be scaled by the volume because there is a dimension mismatch between C_{sca} and the absorption coefficient α. The α-lactose crystal are assumed to be spherical with radius r_{LCT} of 10 μm based on the size of the majority of crystals observed in Fig. 8. The refractive index of α-lactose n_{LCT} is unavailable from FTIR measurements but is estimated to be 1.8 from extrapolated THz-TDS measurements (results not shown). The surface conductivity of α-lactose is assumed to be zero based on milli-Siemens per meter values reported for whole milk [14].

Figure 12 presents the scattering mitigated plots for all samples using the α-lactose parameters. The scattering mitigation technique reduces the baselines for all samples except in the lower frequency range for the 7 mm pellet containing Aldrich PE; this is clearly seen from the solid black line plot in Fig. 13(a). This steep rise in the low-frequency baseline is very similar to that observed in [27], where the authors describe the *Christiansen scattering effect* in pellets containing very large grains (400–600 μm diameter) of DL-phenyllactic acid mixed with PE, measured up till 2.5 THz. In that study, the authors use the refractive index frequency profile of the DL-phenyllactic acid, which was the dominant scatterer, to mitigate the scattering.

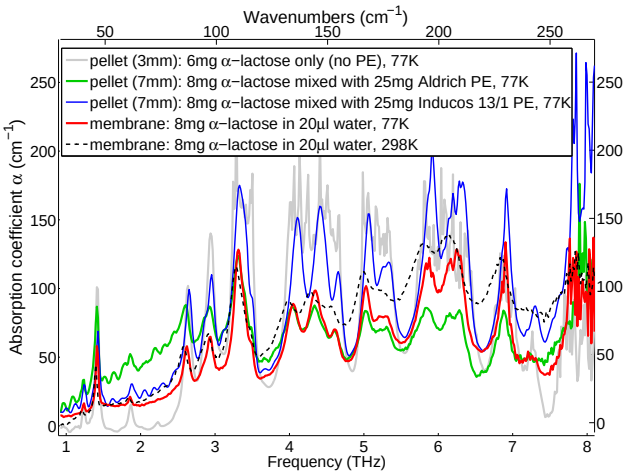

Fig. 12. Plots from Fig 11(a) after scattering mitigation using Mie theory with α-lactose parameters. The rising baselines seen in Fig 11(a) are reduced in this figure, allowing for more accurate representations of the samples' optical properties.

Polyethylene powder is expected to be the dominant scatterer in the 7 mm pellet containing Aldrich PE, thus we use the optical properties of PE instead. Refractive index information across the frequencies of interest is unavailable for FTIR measurements thus we are unable to apply the technique given in [27] on our data. We have instead estimated the refractive index of PE n_{PE} to be a constant 1.54 based on the results presented in Fig. 6(b) and those found in literature for bulk HDPE in the FIR band [13]. The radius of PE is 36 μm for Aldrich PE, and 30 μm for Inducos 13/1 PE based on the SEM studies reported in [3] and the specifications provided by the manufacturers.

The improvement to scattering mitigation using the Aldrich PE parameters is evident from the line-dot plot in Fig. 13(a). A similar improvement is observed in Fig. 13(b) for the 7 mm

#225002 - $15.00 USD Received 15 Oct 2014; revised 22 Dec 2014; accepted 4 Feb 2015; published 18 Feb 2015

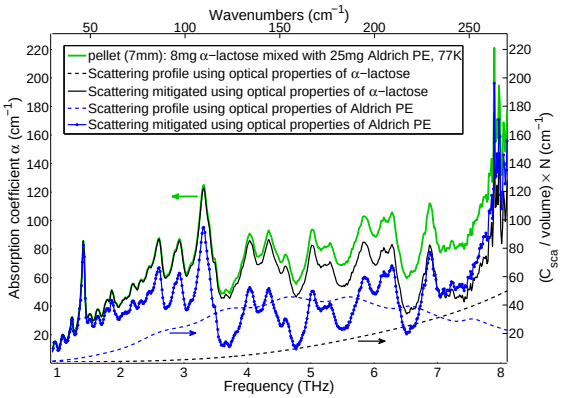

(a) Scattering profiles and mitigation for the 7 mm pellet containing Aldrich PE

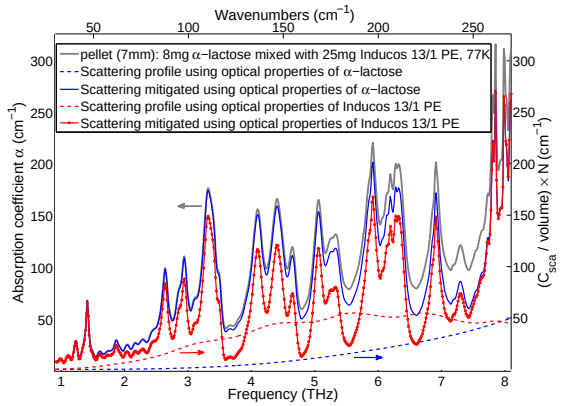

(b) Scattering profiles and mitigation for the 7 mm pellet containing Inducos 13/1 PE

Fig. 13. Scattering profiles used to reduce the rising baselines of the two 7 mm pellet-held samples. The factor $N = 1/20$ is needed to scale the scattering profiles within the limits of α. Modeling scattering with PE as a dominant scatterer yields improved mitigation over that attained in Fig. 12 where α-lactose is assumed to be the dominant scatterer.

#225002 - $15.00 USD Received 15 Oct 2014; revised 22 Dec 2014; accepted 4 Feb 2015; published 18 Feb 2015

pellet containing Inducos 13/1 PE. The steep baseline at low frequencies in Fig. 13(a) is reduced but not completely removed, indicating that mixed pellets may require piecewise removal of scattering by applying different scattering models to different parts of the spectrum.

Unlike samples containing only one test powder, modeling scattering in mixed samples is more complex and may be due to a combination of scatterers. The Mie model we use here is rudimentary and is more appropriate for the samples containing only one test powder, thus we have better scattering mitigation for the NC-held samples. A more thorough investigation into the scattering effects encountered in this work will be reported elsewhere.

5. Conclusion

This study has demonstrated the use of a double-layered NC structure as an alternative sample holder to PE-filled pellets for small quantities of THz/FIR test sample. The double-layered structure provides a good balance between THz transmissivity, sample holding capacity and avoidance of etalon artifacts. At lower THz frequencies, the absorption profile of NC is not as flat as that of PE but is comparable to that of quartz glass; the refractive index of NC is slightly lower than that of PE. At higher frequencies, the absorption profile of NC lies between that of UHMWPE (Aldrich) and HDPE (Inducos 13/1). Furthermore, NC has no obstructive spectral peaks from 0.1 THz to beyond 12 THz.

For quantities of α-lactose below 10 mg, the spectral positions of the peaks obtained from NC-held samples are as accurate as those obtained from pellet-held samples across both the lower (TDS-based measurements) and higher (synchrotron-based measurements) THz frequency ranges. However peaks from the NC-held sample are far superior in terms of clarity and definition to those from the pellet-held sample at lower frequencies. Scattering is prevalent in NC-held samples as evident from the rise in the baselines, but we have shown removal of the scattering artifact is possible using a standard Mie scattering model with estimated optical properties of α-lactose.

The use of NC has allowed us to achieve three important goals that have previously been difficult to attain: *(i)* removing the need for PE hence eliminating the variability caused by PE grain size; *(ii)* significant reduction in sample quantity owing to a reduction in etalon artifacts for the lower THz range, and *(iii)* the direct use of samples in an aqueous medium without a liquid cell for synchrotron-based measurements. Although we are still far from the sub-milligram milestone, we have been able to reduce the quantity of sample used without any need for specially fabricated holders or major changes to either the standard THz-TDS layout or the FTIR system. The NC sample holder is simple, easy to use and is commercially available. The direct use of samples in an aqueous medium has immense benefits for measuring many biochemical samples that exist in solution. The use of NC as a holding medium for aqueous samples under synchrotron-based THz investigation will be the focus of our future work.

Acknowledgments

GMP gratefully acknowledges financial support from the Australian Research Council through grant DE120101494. This work was performed at the University of Adelaide and the Australian Synchrotron; SEM work was performed at Adelaide Microscopy.

#225002 - $15.00 USD Received 15 Oct 2014; revised 22 Dec 2014; accepted 4 Feb 2015; published 18 Feb 2015